ELSEVIER

Journal of Alloys and Compounds 434–435 (2007) 211–214

Journal of ALLOYS AND COMPOUNDS

www.elsevier.com/locate/jallcom

Evolution of lattice parameter and process rates during nanocrystallization of amorphous Fe–Co–Si–B alloy

D.M. Kepaptsoglou [a,*], P. Švec [b], D. Janičkovič [b], E. Hristoforou [a]

[a] *Laboratory of Physical Metallurgy, National Technical University of Athens, 9 Heroon Polytechniou Str., Zografou Campus, 15780 Athens, Greece*
[b] *Institute of Physics, Slovak Academy of Sciences, Dubravska Cesta 9, 845 11 Bratislava, Slovakia*

Available online 4 October 2006

Abstract

The micromechanisms controlling the formation of nanocrystalline phases from an amorphous state were investigated through detailed structural and thermodynamic analysis of phases evolved during crystallization of the amorphous $Fe_{60}Co_{20}Si_5B_{15}$ alloy. Transformation kinetics were determined from electrical resistivity measurements. The structure of the produced phases was quantitatively identified by classical structure analysis. In particular, the lattice parameter of the resulting bcc-FeCo phase was determined for all transformation stages. Kinetic parameters of the phase transformations taking place were calculated by classical kinetic Avrami analysis. The distributions of process rates and activation energies during phase transformations were analyzed. The results are correlated to the presence and content of Si in the produced phase and to the distribution of activation energies active at different stages of the transformation.

Keywords: Metallic glasses; Crystallization kinetics; Phase transformations

1. Introduction

The transformation kinetics in the $Fe_{64}Co_{21}B_{15}$ amorphous system have been investigated in detail in previous work [1]. In particular, short range order and spatial heterogeneities of the amorphous precursor were correlated to a distribution with time and temperature of active crystallization processes. The aim of the present research is to assess the effect of the partial replacement of metallic elements by a small amount of Si on kinetics and process rates of these phase transformations with respect to the evolution of microstructural characteristics. The addition of Si in the relatively simple Fe–Co–B system is attractive because the resulting alloy can serve as a model for understanding the crystallization mechanisms in more complex alloys with composition close to those of Co-containing FINEMET or Si-containing HITPERM.

2. Experimental

A master alloy of composition $Fe_{60}Co_{20}S_{i5}B_{15}$ was prepared from elements with purity better than 99.5%. Amorphous ribbons 10 mm wide and approximately 25 μm thick were prepared by planar flow casting. The composition and amorphous state of the ribbons were verified by inductively coupled plasma spectroscopy and X-ray diffraction, respectively. Phase transformations were monitored by high-precision four-probe electrical resistivity measurements (ER) whose accuracy, including the temperature variations, was better than 0.01%. Measurements were performed on samples in amorphous state, in vacuum, during isothermal annealing at temperatures between 740 and 820 K in increments of 10 K; special design of the annealing furnace allowed a fast settling of the sample temperature and high long-term thermal stability (±0.1 K over 1000 min).

Transmission electron microscopy (TEM) and selected area electron diffraction (SAED) were performed on annealed samples prepared by ion-beam polishing. The X-ray diffraction measurements were performed using Cu Kα radiation with a graphite monochromator in the diffracted beam. The diffractometer goniometer was calibrated using a NIST LaB_6 standard, while single crystal Si was used as an internal standard for each measurement.

3. Structural analysis

The time dependence of the ER (normalized to the value of R for $t = 5$ s) shows a two-step crystallization reaction for all annealing temperatures (Fig. 1). The two sudden drops in resistivity indicate the beginning of the first and second crystallization reactions, respectively. The two crystallization reactions for this particular sample are separate enough in time and temperature that the phase transformation kinetics can be conveniently studied in a single measurement without any significant overlap.

The microstructure and morphology of the samples were analyzed in detail at different crystallization stages. At the very early

* Corresponding author. Tel.: +30 210 7722 127; fax: +30 210 7722 119.
E-mail address: dkepap@mail.ntua.gr (D.M. Kepaptsoglou).

0925-8388/$ – see front matter © 2006 Elsevier B.V. All rights reserved.
doi:10.1016/j.jallcom.2006.08.171

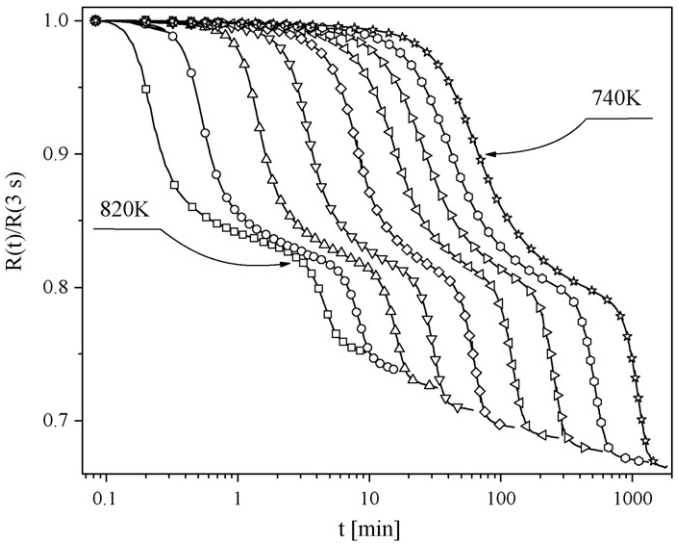

Fig. 1. Time evolution of electrical resistivity for annealing temperatures ranging from 740 to 820 K.

stages of the first crystallization reaction, star-shaped bcc-FeCo particles precipitate in the amorphous material (Fig. 2a). The forbidden reflections of the bcc lattice were identified on the SAED pattern, indicating a certain degree of ordering in bcc-FeCo (α'-FeCo) in the initial stages of transformation. The growth of the bcc-FeCo phase continues with the formation of large dendrites throughout the amorphous matrix (Fig. 2b). By the end of the first crystallization reaction the metallic phase occupies more than 50% of the volume. The SAED pattern was then indexed as α-FeCo: the bcc super-lattice reflections are not present. Further annealing during the second transformation stage leads to the transformation of the inter-granular amorphous matrix into FeCo boride phases (Fig. 2c).

The phases formed during the two crystallization processes were also identified by X-ray diffraction (Fig. 3) for the various steps of the transformation process. By the end of the first stage, the progressive appearance of the bcc-FeCo peaks is observed at the expense of the amorphous lump in the X-ray diffraction pattern. Longer annealing leads to the formation of t-$(FeCo)_3B$ in the second stage which subsequently re-crystallizes into t-$(FeCo)_2B$. The lattice parameter α_{FeCo} of the bcc-FeCo phase was calculated from the angular positions of X-ray diffraction peaks by linear extrapolation, using least squares fitting [2]. During the initial stages of the bcc-FeCo phase formation the value of α_{FeCo} increases from 2.8540 to 2.8567 Å and then decreases to values as low as 2.8540 Å as the transformation progresses. This decrease continues during the second transformation reaction. It has been suggested that an enrichment of the metallic phase with Co and Si could lead to smaller values of the lattice parameter for similar alloy compositions and FINEMET, respectively [3,4].

4. Results and discussion

The time evolution of the ER (Fig. 1) was used to obtain the crystallinity content using a serial resistivity model [1].

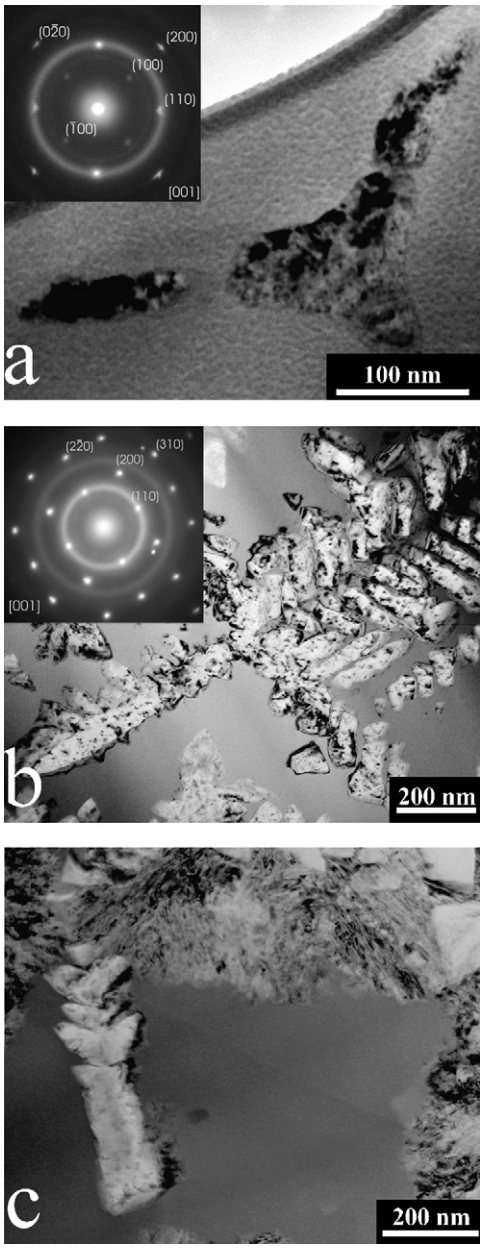

Fig. 2. Microstructure formed after annealing at 760 K for: (a) 3 min, (b) 100 min and (c) 200 min. *Inset*: SAED patterns correspond to the crystalline particles.

Classical Avrami kinetic analysis yields activation energies of ∼300 kJ/mol in a ±50 kJ/mol interval and ∼350 kJ/mol in a ±20 kJ/mol interval for the two crystallization reactions, respectively. Similarly the Avrami parameter ranges from 4 down to 1 during the first reaction and, furthermore, exhibits a strong temperature dependence (Fig. 4). The second stage exhibits a similar behaviour but to a lesser extent, with inverted temperature dependence.

Using the Kristiakova–Svec (KS) approach [1], the rates of processes controlling the transformations were obtained (Fig. 5, bottom). The rates of processes active in the first stage are distributed across a broad interval, while the second stage transformation is characterized by a nearly single-rate value, as reflected by the observed evolution of $x_c(t)$ during this stage (a sharp

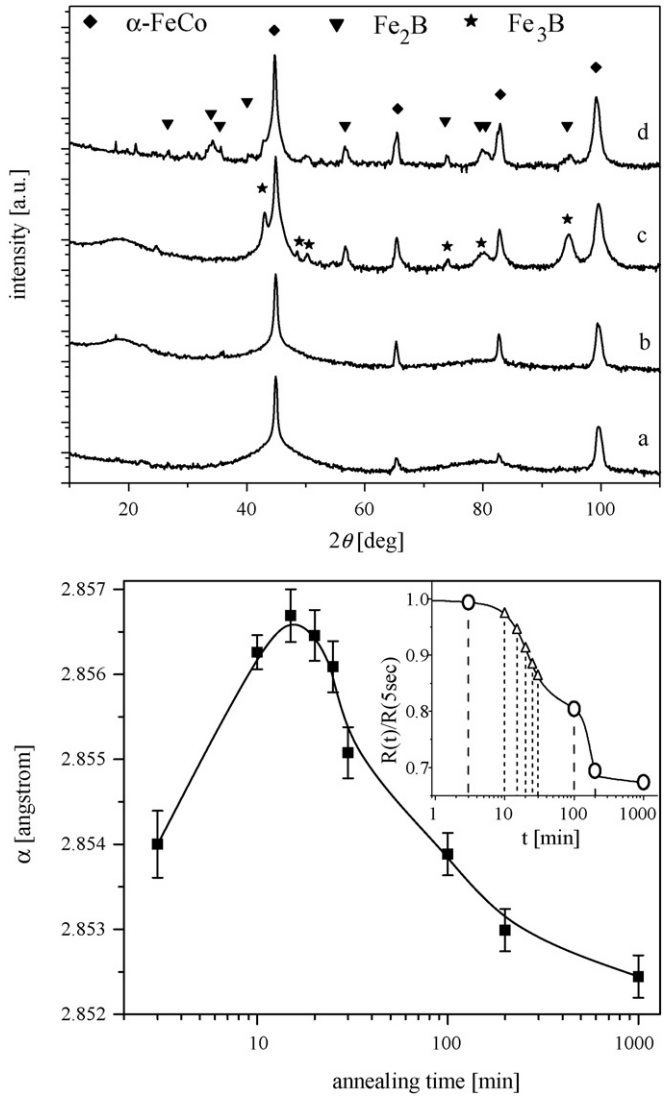

Fig. 3. Top: X-ray diffraction patterns of $Fe_{60}Co_{20}Si_5B_{15}$ samples isothermally annealed at 760 K for 3, 100, 200 and 1000 min (curves a–d), respectively. Bottom: evolution of the lattice parameter of bcc-FeCo for different crystallization stages indicated in the inset.

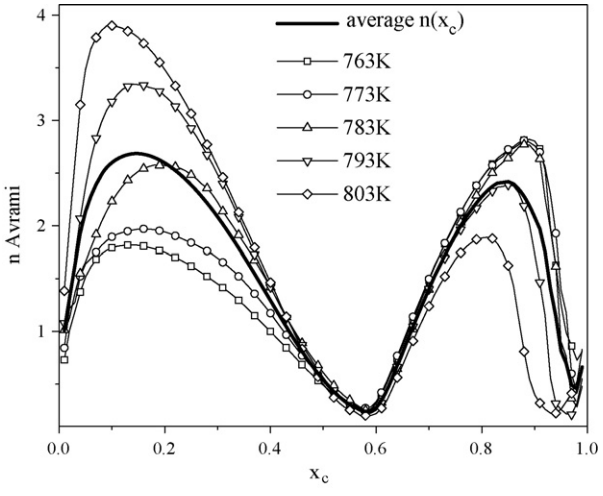

Fig. 4. The evolution of local Avrami parameter with crystallinity for different annealing temperatures.

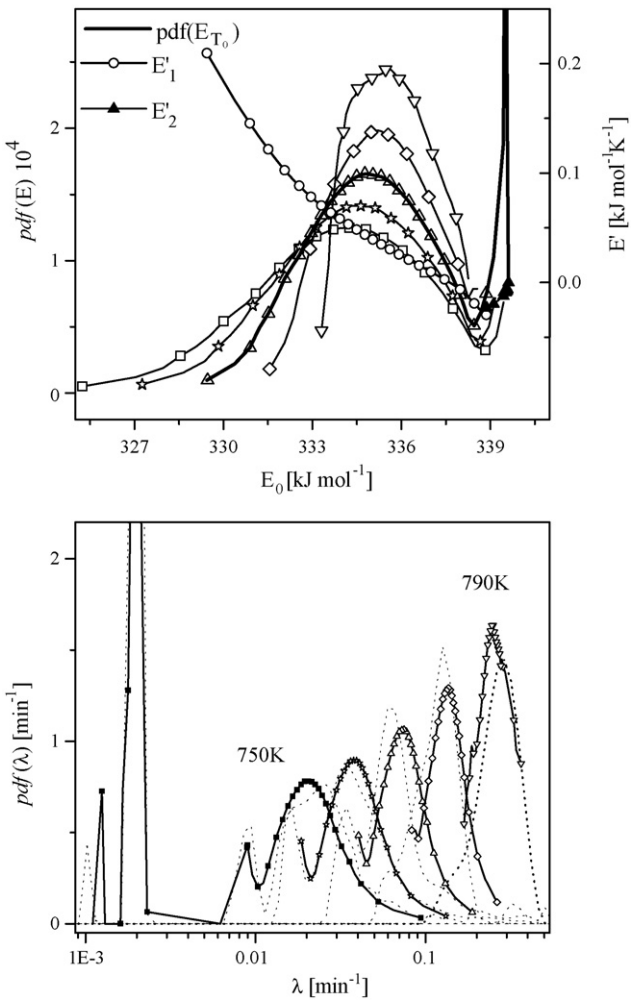

Fig. 5. Top: normalized distributions of activation energies of the two transformation reactions in $Fe_{60}Co_{20}Si_5B_{15}$ for five selected isotherms and the temperature dependence of activation energies $E'(E_0)$. The thick line indicates pdf(E_0) at a mean temperature $T_0 = 770$ K. Bottom: experimental (thin lines) and calculated (lines with symbols) rate distributions for five selected transformation isotherms from Fig. 1.

decrease of ER within a narrow time interval). The distribution of activation energies pdf(E) for all analyzed temperatures presents a narrow ∼6 kJ/mol width around ∼333 kJ/mol, whilst on the other hand that of the second reaction is nearly delta-shaped around ∼339 kJ/mol. The corresponding temperature dependencies of activation energies $E'(E)$ exhibit small positive values for the first reaction but are almost zero for the second reaction, in agreement with the stable value of its activation energy at all annealing temperatures. Higher $E'(E)$ for the first reaction accounts for the spread of effective Arrhenius–Avrami activation energies observed in classical analysis. The values of the pre-exponential factors of the process rates were determined to be true constants for the entire transformation stages, 3×10^{21} and 7×10^{20} min^{-1} for the first and second reaction, respectively. Similarly the Avrami parameter was very exactly a constant 4. The lower value of the pre-exponential factor for the second reaction reflects again the fact that this reaction takes place on a 10 time smaller time scale. The reverse calculations

of the rate distributions, shown for the case of 750 K by solid squares for both transformation reactions in Fig. 5, bottom, fit very well the experimental rate distributions.

While in Si-free $Fe_{64}Co_{21}B_{15}$ no evolution of α_{FeCo} has been observed [1], a drastic change is observed in this case after addition of 5 at.% Si. The low value of α_{FeCo} together with the super-lattice reflection observed in the initial stages suggest the formation of phases enriched in Co from quenched-in clusters with Co/Fe ratio enhanced against the nominal composition. Higher values of $E'(E_0)$ during these initial stages indicate a process with a nucleation-like mechanism, which agrees with the ordering of Fe and Co taking place during crystallization of the originally amorphous Co-enriched clusters. The later stages of the first reaction then involve the remaining metal-rich clusters with higher Si content and with higher thermodynamic stability (activation energies lying above ~332 kJ/mol), which, in turn, decreases further the effective lattice parameter. These considerations agree with a subsequent decrease of the slope of the $E'(E_0)$ in Fig. 5 during the second half of the first reaction indicating a lesser need for nucleation-like rearrangements.

5. Conclusions

In this study, the phase transformations of the amorphous $Fe_{60}Co_{20}Si_5B_{15}$ are presented. The structural analysis revealed a change of lattice parameter of the primary bcc-FeCo phase throughout the two transformation stages. This combined with the presence of super-lattice reflections in SAED patterns reflect an evolution of ordering and composition if the bcc-FeCo phase during crystallization, attributed to enrichment of the latter in Si with ongoing primary crystallization.

The mobility and thermodynamic stability of clusters of the amorphous precursor is related to the presence of Si therein: Si enriched clusters are incorporated in the latter stages of the first reaction, as reflected by the temperature dependence of the activation energy.

Acknowledgments

Acknowledgements are due to the PENED 2001 01ED93 of the Hellenic GSRT, the Slovak GAS (VEGA 5/5096/25, APVT-51-052702, APVT-99-017904 and SO 51/03R8 06 03) and CEX of SAS Nanosmart.

References

[1] K. Kristiakova, P. Svec, Phys. Rev. B 64 (2001) 184202.
[2] B.D. Cullity, S.R. Stock, Elements of X-Ray Diffraction, third ed., Prentice Hall, 2001.
[3] I.C. Rho, C.S. Yoon, C.K. Kim, T.Y. Byun, K.S. Hong, J. Non-Cryst. Solids 316 (2003) 289.
[4] K. Hono, J.L. Li, Y. Ueki, A. Inoue, T. Sakurai, Appl. Surf. Sci. 67 (1993) 398.